The Impact of Thermal Degradation on Properties of Electrical Machine Winding Insulation Material

Malgorzata Sumislawska, Konstantinos N. Gyftakis, *Member, IEEE*, Darren F. Kavanagh, Malcolm D. McCulloch, *Senior Member, IEEE*, Keith J. Burnham, and David A. Howey, *Member, IEEE*

***Abstract*—Interturn stator short circuits can develop quickly leading to serious damage of an electric machine. However, degradation mechanisms of winding insulation material are not yet fully understood. Therefore, the main contribution of this paper is the analysis of the impact of thermal ageing on the electrical properties of the thin-film winding insulation. The insulation samples have been aged thermally at 200 °C–275 °C and for 100–1600 h. After ageing, impedance spectroscopy measurements were undertaken on the samples and equivalent-circuit model (ECM) parameters fitted for each measurement. This allows the impact of thermal ageing on ECM parameters to be analyzed, giving insight into the changes in the electrical properties of the insulation. Finally, high voltage was applied to the samples aiming to identify the breakdown-voltage (BV) characteristics of the insulation material.**

***Index Terms*—Electric machine, equivalent-circuit model (ECM), impedance spectroscopy, polyamide-imide (PAI), stator winding, thermal degradation.**

I. Introduction

STATOR faults are an important cause of electrical machine failures. The appearance of stator faults depends on the size of the electrical machine. According to [1], low-voltage induction motor stator faults account for only 9% of total failures. In medium-voltage induction motors, the percentage increases to 35–40%, whereas for high voltage, it is more than 65% [2]–[6]. Among all possible stator faults, interturn stator faults are of particular interest, because they are challenging to detect, especially at low severity levels [7]–[10], however, they can evolve quickly leading to serious motor damage [11]. Moreover, these faults are difficult to discriminate from stator voltage supply imbalances. As a consequence, a variety of fault detection techniques including neural networks and envelope analysis have recently been applied [12]–[17].

Alternatively, other researchers have tried to directly understand the physical mechanisms that lead to insulation degradation [18], leading to lifetime prediction and machine life prognosis models that may be used to improve the performance and reduce the cost. It is now well known that there are many different ageing stresses: electrical, thermal, mechanical, humidity, moisture, etc. [19]. There have been many studies aimed at understanding insulation thermal ageing. An effort is made here to review and summarize some important past contributions.

First, it has been noted that, online thermal and chemical monitoring techniques are cost effective only in large machines [20]. Moreover, protective relays are triggered after the insulation has been seriously damaged and thus they cannot be considered to help toward the monitoring of the fault especially at low severity levels [21].

Furthermore, there are a variety of techniques that deal with the ageing mechanisms of the electrical machine winding insulation. In [22], a significant resin weight loss was observed around the winding in a failed induction motor. In addition, it was found in [23] that after the initial ageing cycles, there was a shift of the dissipation factor and the capacitance at all voltage levels toward lower losses and capacitances because of the drying out and postcuring of the insulation. Moreover, a new life span model was developed in [24], which presents an original relationship between the insulation life span and the stress parameters with the application of the design of experiments (DoE) methodology. Also, in [25], a new cable-monitoring method was proposed based on impedance spectrum analysis in the high-frequency range. Furthermore, in [26], the authors used a regression tree constructed with 32 experiments for insulation lifespan modeling (twisted pairs). One of their findings is that at low voltages, only the temperature has a significant effect on the lifespan. In the same work, in parametric DoE and response surface (RS) models, the lifespan is expressed as a linear additive function of the predictors and their effects. The most influent factors and interactions were identified as those having the highest estimated effects: the voltage V, the temperature T, their interaction, and the T^2. Finally, in [27], the authors experienced a 20% capacitance drop of their tested windings after five thermal cycles. In the same work, they proposed a method that is based on the monitoring of the current

Manuscript received September 9, 2015; revised November 24, 2015 and February 2, 2016; accepted March 5, 2016. Date of publication March 21, 2016; date of current version July 15, 2016. Paper 2015-EMC-0766.R2, presented at the 2015 IEEE International Symposium on Diagnostics for Electrical Machines, Power Electronics, and Drives, Guarda, Portugal, September 1–4, and approved for publication in the IEEE Transactions on Industry Applications by the Electric Machines Committee of the IEEE Industry Applications Society.

M. Sumislawska is with the Department of Mechanical Automotive and Manufacturing, Coventry University, Coventry, CV1 5FB, U.K. (e-mail: malgorzata.sumislawska@coventry.ac.uk).

K. N. Gyftakis is with the Department of Computing, Electronics, and Mathematics, Coventry University, Coventry, CV1 5FB, U.K. (e-mail: k.n.gyftakis@ieee.org).

D. F. Kavanagh is with the Department of Electronic, Mechanical and Aerospace Engineering (EMA), Institute of Technology Carlow, Carlow, R93 V960, Ireland (e-mail: Darren.Kavanagh@itcarlow.ie).

M. D. McCulloch and D. A. Howey are with the Department of Engineering Science, University of Oxford, Oxford, OX1 3PJ, U.K. (e-mail: malcolm.mcculloch@eng.ox.ac.uk; david.howey@eng.ox.ac.uk).

K. J. Burnham is with Department of Mechanical, Automotive and Manufacturing Engineering, Coventry University, Coventry, CV1 5FB, U.K. (e-mail: k.burnham@coventry.ac.uk).

Color versions of one or more of the figures in this paper are available online at http://ieeexplore.ieee.org.

Digital Object Identifier 10.1109/TIA.2016.2544745

transients after step-voltage excitation applied by the inverter and was applied on a high-voltage induction motor.

In the above papers, the most commonly applied degradation technique is that of accelerated ageing, which deserves some further explanation. It has been reported in [25] that unstrained tests give overly optimistic information relating to long-term design data or predictions of expected lifetime. Furthermore, this type of testing has limitations. If the applied temperature exceeds some critical value, then different chemical reactions are caused compared to the real ageing mechanisms. However, in [26], the application of multistress ageing on stator bars was successful in predicting the real ageing mechanisms of actual bars in applications working for 22 years. In the same work, the significant role of mechanical stress is highlighted because the loosening of the stator bars in the slots leads to vertical vibrations that enhance the degradation mechanism.

Most of the research in the topic of electric machine insulation degradation focuses on the behavior of the whole winding or twisted pair samples. Due to the nature of such research, the insulation is subjected to multiple types of stress at once (thermal, mechanical, etc.). However, not much attention has been paid to the properties of the insulation material itself. Therefore, in this paper, we investigate the properties of thin-film insulation material subjected to an isolated thermal stress. Thus, the research presented in this paper supplements the work on more complex geometries, such as the twisted pairs and the windings.

The results presented in this paper are the part of an ongoing study of the impact of thermal degradation on the properties of thin-film insulation material. The work presented in this paper is a continuation of our research described in [31]. This paper is organized as follows. Section III provides the estimation accuracy for resistance and capacitance measurements. In Section IV, the dielectric measurements of new (unaged) samples are analyzed to verify the consistency of dielectric properties of new samples (this allows to determine the manufacturing quality of new insulation samples and forms a baseline for degradation analysis). In Section V, the variations of insulation dielectric properties as for different temperatures are analyzed to a greater extent than in [31]. Finally, the breakdown-voltage (BV) characteristics of the tested samples after the application of high-voltage stress are illustrated in Section VI leading to a development of a BV model as a function of temperature.

II. Experiment Design

Sample specimens were prepared from industrial grade class H, polyester 200 rectangular enamel wire (IEC 60317-29 standard). The rectangular wire ($15.5\ \mathrm{mm} \times 2.5\ \mathrm{mm}$) was cut into specimens that were 350-mm long. Both ends of the specimens were drilled for making electrical connection points for dielectric measurement purposes. One hundred and eighty of these polyamide-imide (PAI) insulation samples were then divided into six groups of 30 samples each. Each group of samples was placed into separate laboratory thermal chambers. These chambers were set to temperature set points of 200 °C, 215 °C, 230 °C, 245 °C, 260 °C, and 275 °C, respectively. Each group of samples that were aged at the same temperature was further divided into five subgroups of six samples each. Each subgroup was aged for a different period of times at a fixed temperature, these ageing time durations were 100, 200, 400, 800, and 1600 h, respectively. After the thermal ageing, samples were placed in specially fabricated plastic holders and the impedance responses were measured at six equally spaced points 40 mm apart along the sample specimens using a dielectric-probe test fixture (the parallel-plate method [28]). The impedance measurement equipment used was the N4L PSM1735 Impedance Analyzer using a dielectric probe based on the standard ASTM D150-11. The impedance measurements (C, DF, |Z|, and Θ) were made over the frequency range 1 Hz to 20 MHz.

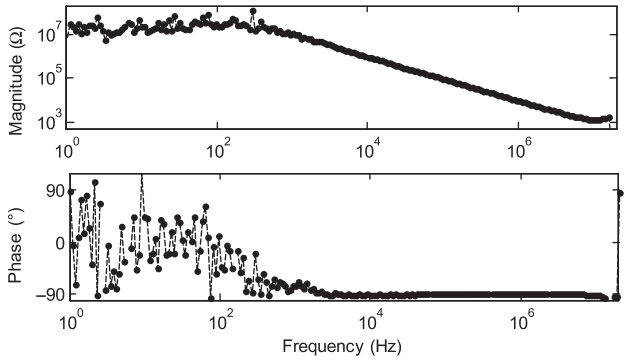

Fig. 1. Impedance spectroscopy of insulation sample.

Furthermore, the impedance spectroscopy of 20 new (i.e., unaged) insulation samples was carried out in the same manner for comparison with the aged samples. Further details of the experiment design can be found in [31].

III. Equivalent-Circuit Model

Impedance spectroscopy of an example insulation sample is presented in Fig. 1. The insulation exhibits a capacitive behavior for frequencies above 1 kHz, while for frequencies below 1 kHz, the impedance is mainly resistive.

The insulation impedance response has been modeled using an equivalent-circuit model (ECM) comprising a capacitor *C* and resistor *R* connected in parallel

$$Z(j\omega) = \frac{R}{RCj\omega + 1} \tag{1}$$

where ω is the frequency expressed in radians per second and $j = \sqrt{-1}$. The *R* and *C* parameters of the ECM have been fitted and histograms of parameters of new samples are plotted in Fig. 2. Estimation uncertainties [assuming 95% confidence bounds (see [32] for more details)] of *R* and *C* are analyzed in the following sections.

A. Uncertainty of Resistance Estimation

Fig. 3 presents the uncertainty of the resistance estimation, denoted δR, versus the fitted value of resistance for all measurements of the unaged samples. It is observed that the resistance estimation uncertainty is proportional to the value of resistance *R* and has been obtained with $\delta R/R \cong 19\%$ accuracy on average. A similar observation has been made with respect

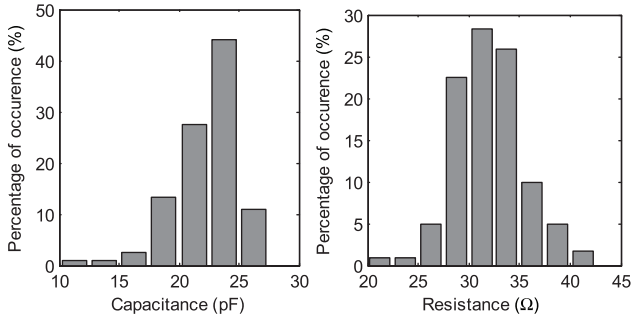

Fig. 2. Histograms of capacitance and resistance of unaged insulation.

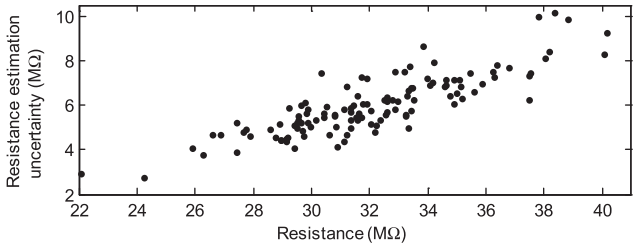

Fig. 3. Uncertainty of resistance estimation versus resistance estimate.

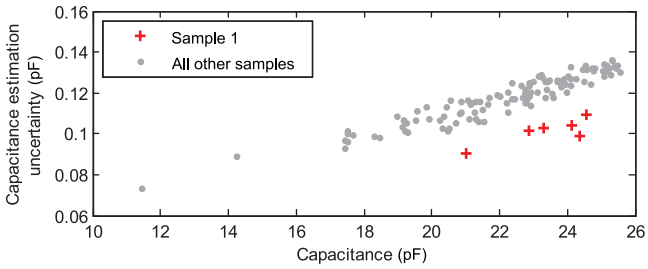

Fig. 4. Uncertainty of capacitance estimation versus capacitance estimate.

to the aged insulation samples. This relatively high uncertainty is due to the significant levels of measurement noise observed at low frequencies [where behavior of the insulation is resistive (see Fig. 1)] caused by the inability of the measurement equipment to drive the extremely small currents required for the measurements in this range.

B. Uncertainty of Capacitance Estimation

The uncertainties of the capacitance estimation of the unaged samples, denoted δC, are presented in Fig. 4. For most of the cases, it occurs that $\delta C/C \cong 0.5\%$.

Interestingly, the estimation uncertainty of all points on a single sample (sample 1 in Fig. 5) is slightly lower than the one of other samples.

IV. Analysis of Unaged Insulation

In this section, the consistency of the insulation manufacturing quality is analyzed. It is expected that the impedance measurements taken from each sample (note that, the impedance has been measured as six equally spaced points at each sample) are characterized by comparable mean and standard deviation values. For visual inspection purpose, measurements of

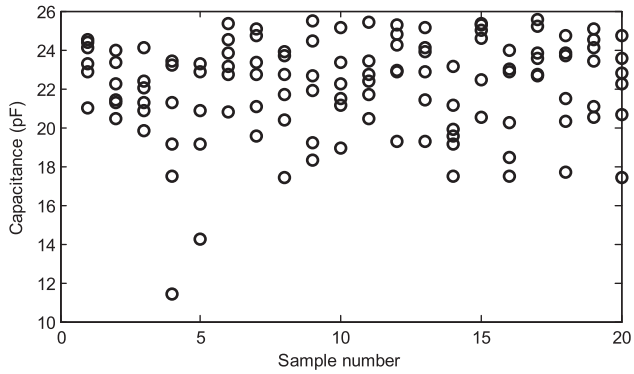

Fig. 5. Comparison of capacitance values measured at each sample.

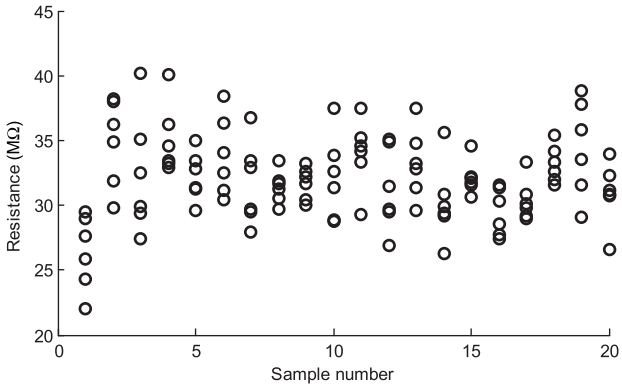

Fig. 6. Comparison of resistance values measured at each sample.

TABLE I
MEAN VALUE (μ_i) AND STANDARD DEVIATION (σ_i) OF SIX ESTIMATED CAPACITANCE VALUES (IN PICOFARADS) FOR EVERY SAMPLE

i	**1**	**2**	**3**	**4**	**5**	**6**	**7**
σ_i	1.3	1.3	1.5	4.5	3.5	1.6	2.1
μ_i	23.3	22.1	21.7	19.3	20.5	23.3	22.7
i	**8**	**9**	**10**	**11**	**12**	**13**	**14**
σ_i	2.4	2.8	2.1	1.7	2.2	2.1	1.9
μ_i	21.6	22.0	22.1	22.7	23.2	22.8	20.1
i	**15**	**16**	**17**	**18**	**19**	**20**	
σ_i	2.0	2.7	1.2	2.7	1.9	2.6	
μ_i	23.9	21.0	23.9	21.9	23.1	21.9	

capacitance and resistance of all new samples are presented in Figs. 5 and 6, respectively. As the capacitance estimate is significantly less affected by measurement noise inaccuracies than the resistance estimate, the capacitance estimates have been used to assess the consistency of the manufacturing quality.

First, the variance of the capacitance measurements taken for each sample has been considered. For every sample, the mean value and standard deviation, denoted by μ_i and σ_i, respectively, of the six measured capacitance values have been calculated (the subscript i denotes the sample number). These are presented in Table I.

Subsequently, for every pair of samples i and j, a hypothesis that $\sigma_i = \sigma_j$ has been tested with the probability level of 0.05 (see [33]). (Also, all further hypotheses have been tested with the probability level 0.05). This hypothesis has been

rejected for some pairs (*i, j*), namely, (1,4), (2,4), (3,4), (4,6), (4,11), (4,17), and (5,17). In order to eliminate the number of potential false positives, Benjamini and Hochberg (BH) correction has been applied. Multiple hypothesis that all pairs (4, *i*), $i = 1, \ldots, 3, 5, \ldots 20$, have equal variances has been carried out applying BH correction with a false discovery rate of 0.05. Subsequently, the test has been repeated for all pairs (17, *i*), $i = 1, \ldots, 16, 18, \ldots, 20$. The hypothesis has not been rejected for any of the pairs; hence, it can be concluded that all samples have equal variance of capacitance values.

Then, the procedure has been repeated to assess whether all samples are characterized with equal mean value. The multiple hypothesis that pairs (14, *i*), $i = 1, \ldots 13, 15, \ldots, 20$ have equal mean with application of the BH correction indicated that samples 14 and 17 have distinct mean value. However, considering that false discovery rate is $\delta = 0.05$ it is expected that in 5% of the cases, the hypothesis may be erroneously rejected.[1] Consequently, it is concluded that the capacitance of new samples can be characterized by a single distribution with the mean values of 22.17 and a standard deviation of 2.46.

V. Aged Insulation

We observed previously [31] that the capacitance of the majority of aged insulation samples is lower than 20 pF regardless of the length of ageing time. The only exceptions from this rule were insulation samples aged at 230 °C, where the capacitance drops from 22–24 pF to around 14 pF between 200 and 800 h of ageing. Based on these observations, a preliminary conclusion is made that the reduction in capacitance to $C < C_d \approx 20$ pF is an indicator of a thermal degradation, which is, however, not an end-of-life condition. (Note that for 18% of new insulation samples $C < 20$ pF, thus the absolute capacitance cannot be a sole indicator of degradation.) Furthermore, the degradation mechanism seems to be dependent on the temperature at which the material is aged, which is indicated by different capacitance of samples aged at 230 °C.

As the most pronounced variations in the electrical properties of insulation were observed in the case of ageing at 230 °C, these results are presented first in Section V-A. Sections V-B and V-C analyzes both the resistance and capacitance of the insulation aged at the other temperatures, respectively.

A. Thermal Ageing of Insulation at 230 °C

Fig. 7 presents the insulation capacitance as a function of time spent at 230 °C, denoted by *t*. Mean values and standard deviations of the insulation capacitance for different values of *t* are presented in Table II.

The capacitance appears to decrease with time. However, this relationship is nonlinear. Also, note that the capacitance of the unaged insulation is 24.0 ± 0.6 pF, which is close to the capacitance of insulation aged at 230 °C for $t \leq 200$. We, therefore, hypothesize that a certain degradation phenomenon occurred between 200 and 800 h leading to the capacitance drop from around 22–24 pF to around 14 pF (note that the occurrence of this mechanism is not an end-of-life condition).

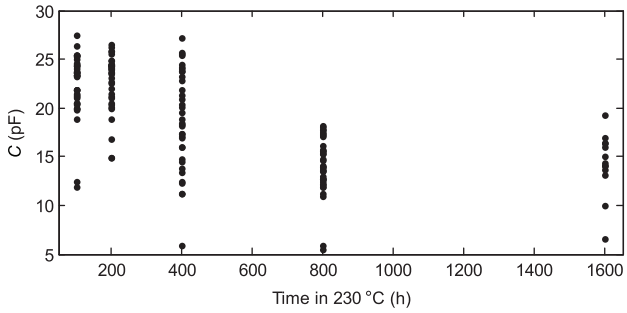

Fig. 7. Capacitance as a function of time for insulation aged in 230 °C.

TABLE II
Mean and Standard Deviation of Capacitance

Time, *t* (h)	100	200	400	800	1600
Mean (pF)	22.4±1.1	22.7±1.0	18.9±1.7	14.2±1.0	14.3±1.8
Standard deviation (pF)	3.3 (2.2–4.8)	2.9 (1.9–4.3)	5.0 (3.3–7.4)	3.0 (2.0–4.4)	3.2 (1.7–6.6)

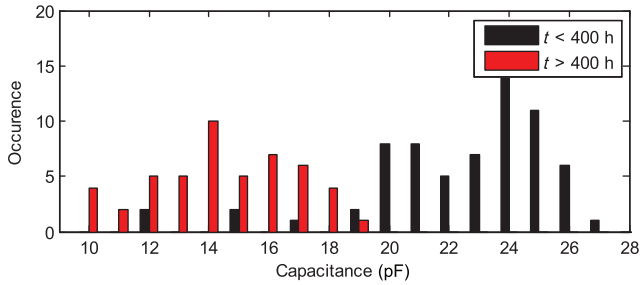

Fig. 8. Comparison of capacitance histograms for ageing time greater and lower than 400 h.

Fig. 8 compares the histograms of capacitance measurements for ageing times greater and lower than 400 h, i.e., before and after the aforementioned ageing phenomenon occurred. It is observed that the distribution of capacitance for $t < 400$ is negatively skewed. However, bearing the results from Section IV in mind, it is assumed in the further analysis that the relatively low capacitance values obtained for $t < 400$ are due to the manufacturing differences rather than thermal ageing. The distributions of capacitance values for $t < 400$ and $t > 400$ have been approximated with the normal distributions $\mathrm{N}(23.1, 4.8)$[2] and $\mathrm{N}(14.2, 9.1)$, respectively, where $\mathrm{N}\left(\mu, \sigma^2\right)$ denotes the normal distribution with mean μ and variance σ^2. These are presented in Fig. 9.

Subsequently, a decision boundary $C_d = 19.1$ pF has been calculated for which the capacitance probability density functions for the two considered cases ($t < 400$ h and $t > 400$ h) are equal. Thus, it is further assumed that the decrease in the capacitance below 19.1 pF indicates that the aforementioned degradation phenomenon has occurred.

[1]The *p*-value is in the equal mean test (*t*-test) of samples 14 and 17 is 0.002 which is close to $\delta \frac{1}{19} = 0.0026$.

[2]In the case of $t < 400$, four measurements with capacitances lower than 15 pF have been excluded from the estimation.

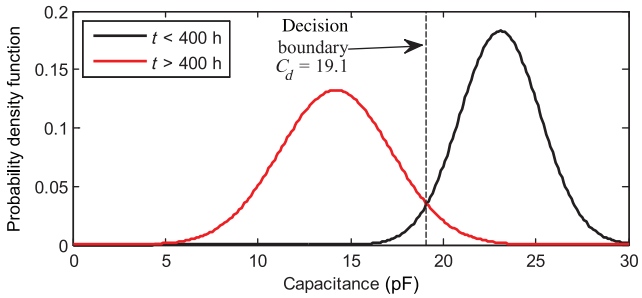

Fig. 9. Gaussian approximation of capacitance distributions for ageing time greater and lower than 400 h.

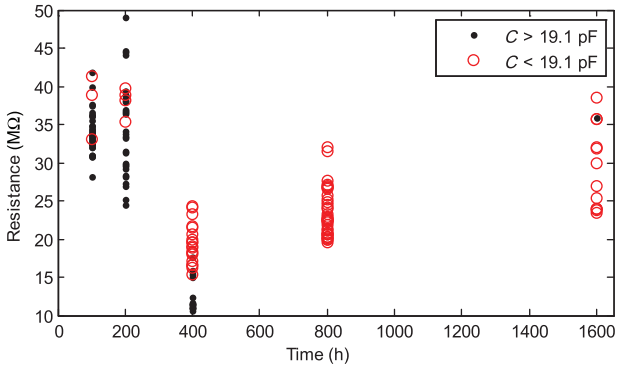

Fig. 10. Insulation resistance as a function of time of ageing at 230 °C. Measurements for which capacitance exceeds 19.1 pF are denoted by red dots, while points for which $C < C_d$ are denoted by black circles.

Fig. 10 presents the insulation resistance as a function of time of ageing at 230 °C. It is observed that for the first 400 h, the resistance decreases. (Note that, the uncertainty of the resistance estimation increases with *R*, and that the four outliers visible in Fig. 10 for $t = 200$ h, for which the estimated resistance is greater than 44 MΩ, have an estimation uncertainty of 11.7 MΩ on average, while the average estimation uncertainty for the remaining measurements for $t = 200$ h is 6.7 MΩ.) Subsequently, after 400 h of ageing, the resistance reaches its minimum (the average resistance estimation uncertainty for $t = 200$ h is 2.1 MΩ), then the resistance increases.

Furthermore, after 400 h of ageing, there is a clear separation between the resistance of 17 points with $C > C_d$ and 19 points for which $C < C_d$ (see Fig. 10). This is also visible in Fig. 11, where the measured capacitance has been plotted against resistance for $t = 400$ h.

The differences between the electrical properties of different points measured at a single insulation sample aged at 230 °C for $t = 400$ are much smaller than the differences between the measurements taken at different samples (see Fig. 11). This could be due to the differences between insulation samples due to manufacturing quality. Therefore, it is expected that the whole area of an insulation sample ages at approximately the same rate, whereas degradation rates may differ among insulation samples. It is observed that the capacitance measured at samples 1–3 aged for 400 h is greater than C_d (except for a single point in sample 3 that has a capacitance of 18.4 pF which is close to 19.1 pF), while the capacitance of samples 4–6 is lower than C_d.

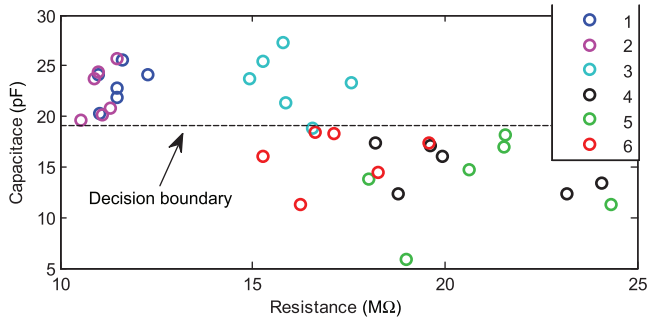

Fig. 11. Resistance and capacitance of insulation aged for 400 h at 230 °C. Different colors denote the measurements taken from different samples.

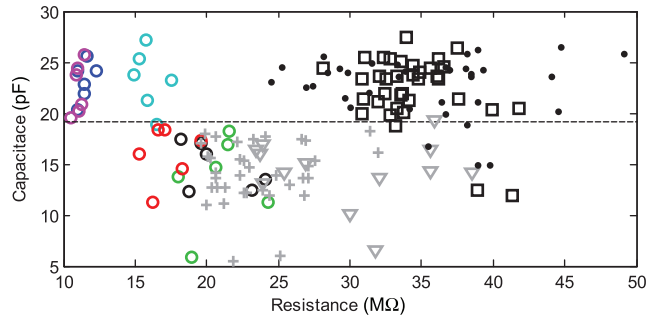

Fig. 12. Electrical properties of insulation with respect to ageing time at 230 °C. Black squares: $t = 100$ h, black dots: $t = 200$ h, gray crosses: $t = 800$ h, gray triangles: $t = 1600$ h, and colored circles: $t = 400$ h (see Fig. 11).

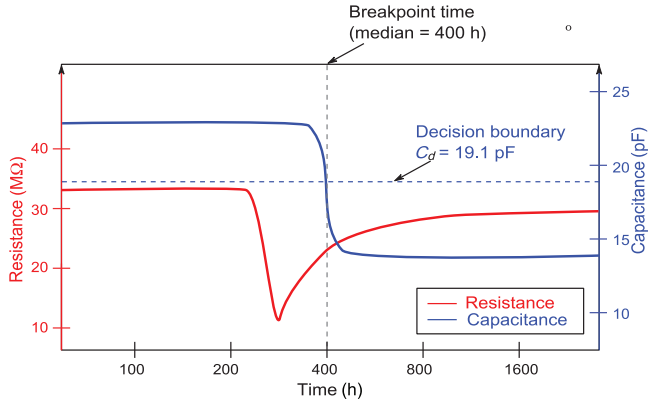

Fig. 13. Schematic of the electrical properties of insulation samples aged at 230 °C.

Fig. 12 compares the resistance and the capacitance of insulation for $t = 400$ with the electrical properties of the insulation aged for times less than and more than 400 h. Comparing Figs. 11 and 12, the following degradation mechanism is observed: for the first 200 h of ageing at 230 °C, no significant change in electrical properties of insulation is noted; the expected values of the resistance and the capacitance of insulation are ≈ 35MΩ and ≈ 23 pF, respectively. Then, the resistance drops to $R_{\min} \approx 11$MΩ. Following the rapid reduction in resistance, the capacitance drops to the expected values of ≈ 14 pF, while the resistance slowly increases. This process has been summarized in Fig. 13, where changes in both resistance and capacitance are plotted against time.

In this regard, it can be assumed that among the six samples aged for 400 h (Figs. 11 and 12), degradation of sample 3 is the least advanced; samples 1 and 2 are at a similar stage of ageing and their capacitance is likely to reduce, while degradation of sample 5 is most advanced.

Note that the exact mechanism of ageing is not known at this stage, and further examination of the chemical properties of the aged insulation material is required to validate the above empirical results. In addition, the resistance and capacitance values in the above degradation results are provisional and approximate. For example, since the measurements are taken every several 100 h, it is not known whether $R_{\min} \approx 11\ \mathrm{M}\Omega$ is the minimum resistance throughout the degradation period.

B. Thermal Ageing of Insulation at $T < 230\,^{\circ}C$

In this section, thermal ageing of insulation at $T = 200\,^{\circ}\mathrm{C}$ and $T = 215\,^{\circ}\mathrm{C}$ is considered. It is observed that the insulation capacitance does not depend on the time of ageing (mean value of 14.5 pF and standard deviation of 2.7 pF). Thus, it is concluded than during the first 100 h of ageing, the capacitance has dropped from approximately 22 pF to around 14 pF. Analogously to the procedure presented in Figs. 8 and 9, distribution of the capacitance of unaged samples has been compared with the capacitance distribution of insulation aged in $T < 230\,^{\circ}\mathrm{C}$ and the decision boundary $C_d = 18.8$ pF has been obtained.[3]

On the contrary, the resistance varies with time. The resistance of the insulation aged at 215 °C first drops and then increases (see Fig. 14). A similar observation has been made with respect to ageing at 230 °C; however, without chemical analysis of the aged samples, it is not known whether these similar observations are due to the same phenomenon. Furthermore, the fact that the capacitance behaves differently at 230 °C suggests that these might be different phenomena.

Note that in the case of insulation aged at 200 °C for 400 h (Fig. 14), there is a significant spread of resistance. Fig. 15 compares the resistance values measured at different samples (aged at 200 °C for 400 h). It is observed that the relatively large spread of resistance values is due to sample 6 in Fig. 15, whose resistance measurements were all relatively low. This might be an outlier, or sample 6 is at a different stage of the ageing process than samples 1–5. Comparing Figs. 10 and 14, we can draw a hypothesis that the ageing process at 200 °C is slightly slower than ageing at 230 °C. It appears that the "dip" of the material resistance visible in Fig. 10 after 400 h of ageing in 230 °C happened in the case of sample 6 in Fig. 15 (i.e., the six lowest resistance measurements for 400 h in Fig. 14), and is yet to happen for the rest of the samples aged in 200 °C for 400 h.

C. Thermal Ageing of Insulation at $T > 230^{\circ}C$

The resistance of insulation aged at higher temperatures than 230 °C exhibits different behavior compared to the previous cases (see Fig. 16). First, all insulation samples were catastrophically destroyed after 1600 h at 245 °C and 260 °C, and

[3]Samples 4 and 5 (see Fig. 5) have been excluded from this calculation.

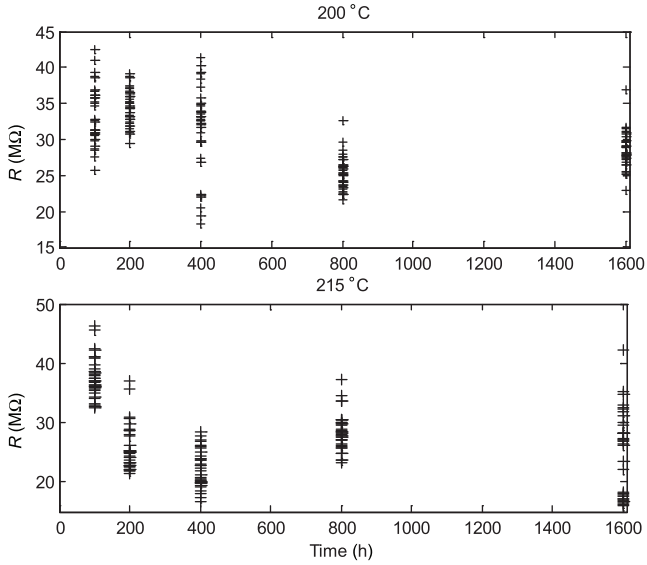

Fig. 14. Resistance of insulation aged in 200 °C and 215 °C as a function of time.

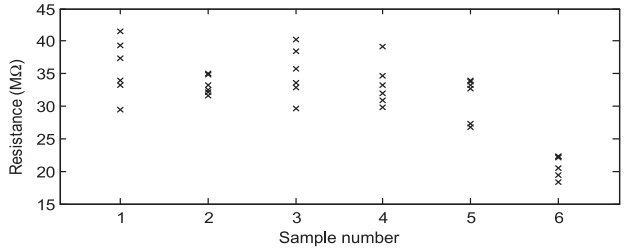

Fig. 15. Resistance of different insulation samples aged at 200 °C for 400 h.

800 h at 275 °C. It has also been observed that during ageing at high temperatures, the insulation delaminates, which leads to increased resistance readings (see Fig. 16). (Note that the resistance reading of a delaminated sample corresponds to the combined resistance of insulation material and the air gap between the material and the electrode. Thus, it is not representative of the material itself.) Reduction in resistance after 800 h at 260 °C is probably due to the fact that the insulation was partially burned; hence, it becomes thinner.

Similar to the low-temperature case, the capacitance does not vary with ageing time (for $T = 245$, 260 °C, the mean value and standard deviation are 14.8 and 2.8, respectively). In the case of ageing at 275 °C, the capacitance is slightly elevated (mean value: 17.3 and standard deviation 2.7), yet it does not depend on the ageing time.

VI. BV Characteristics

An important aspect of prognosis area is to relate the physical properties of a component to the remaining useful life. In this work's case, the remaining useful life is strongly related to the BV of the thin-film insulation material. This is because when the thin-film insulating capabilities decrease, there will be a developing current penetrating the thin film and leading eventually to interturn short circuits.

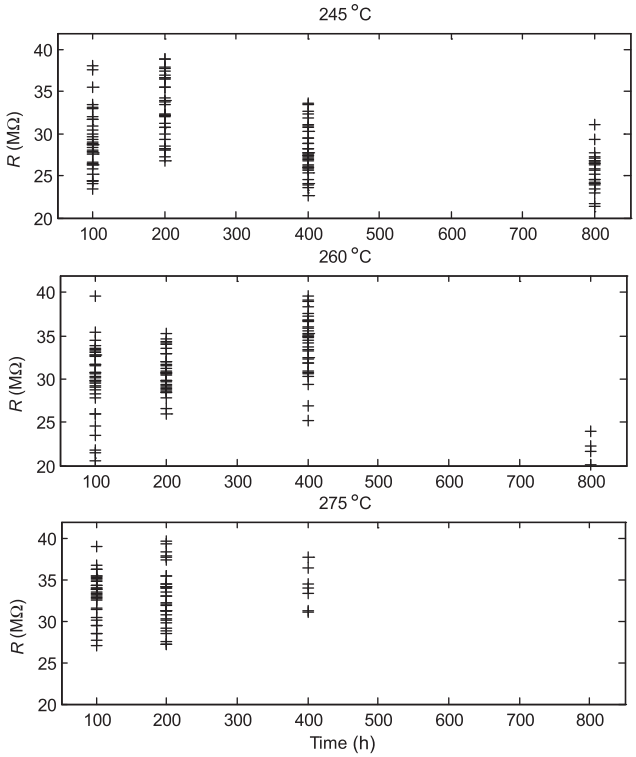

Fig. 16. Resistance of insulation aged at 245 °C, 260 °C, and 275 °C as a function of time.

The early BV (EBV) was measured using the conductive tape approach as defined in the standard CEI EN 60851-5. To make these measurements, a CA6555 Chauvin-Arnoux 15-kV Megohmmeter was used. The sample was placed in a dielectric case and four conducting aluminum tapes are attached to its surface [Fig. 17(a)]. The case is then closed [Fig. 17(b)], so that there are no leakage currents/discharges between the electrodes and/or the sample.

Then, the two high-voltage electrodes are connected to the sample. One is connected at the end side of the copper bar inside the insulation, whereas the second is connected to one aluminum tape at a time [Fig. 17(c)]. The full setup is shown in Fig. 17(d). An optic cable was used to connect the Megohmmeter with a PC controlling the experiment and collecting the data, for safety reasons.

When the connections are ready, the Megohmmeter is set to produce voltage ramps starting at 500 V and ending at 15 kV. The duration of the ramp is 13 min. When the breakdown takes place, the applied high voltage is immediately shut down and its instantaneous value is monitored and stored.

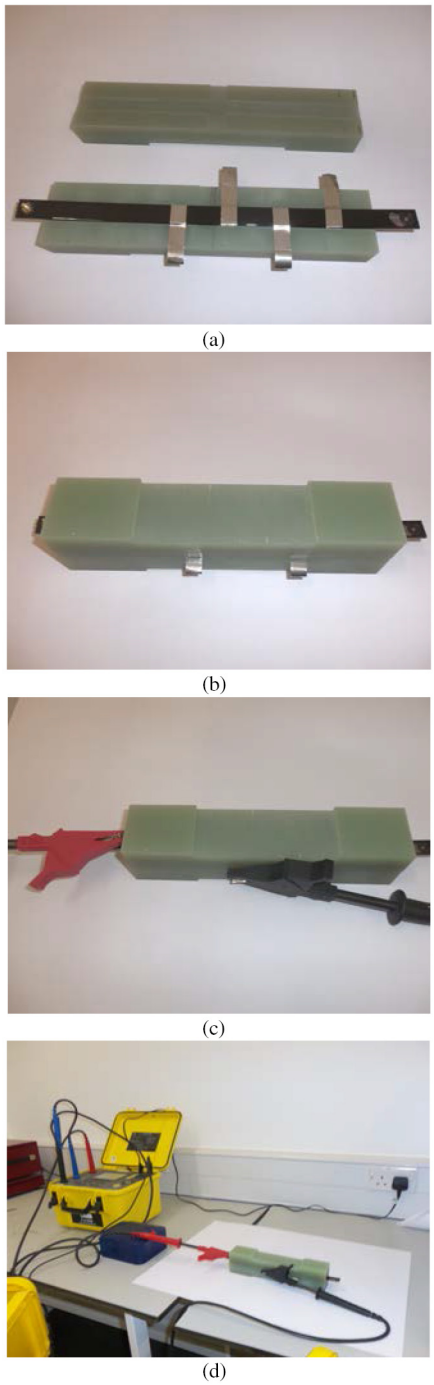

Fig. 17. Preparation of the samples for the BV testing. (a) Attaching the aluminum tape strips. (b) Shielding the sample. (c) Connecting the high-voltage electrodes. (d) Full setup.

A. Analysis of BV Measurements

Tables III and IV present, respectively, the mean and standard deviations of BV measurements of insulation samples aged at different combinations of temperatures and times. In addition, Table V presents the median values of BV for each combination of temperature and time. Mean values of BV measurements for considered combinations of temperature and time (and the 95% confidence bounds of mean estimation) are presented in Fig. 18.

A strong dependency between the ageing temperature and BV has been observed. However, no statistically significant difference has been observed between the insulation samples aged for the same time at different temperatures. Furthermore, it is observed that the standard deviation of BV of new (unaged) samples is significantly greater than the standard deviation measured in aged insulation samples. The standard deviation of BV measurements also appears to reduce as with an increase in ageing time. Fig. 19 compares the histograms of BV measurements

TABLE III
MEAN VALUES OF BV (KV)

		Temperature (°C)			
		200	215	230	All temperatures
Time (h)	100	7.56 (7.14–7.94)	8.15 (7.44–8.86)	7.76 (7.12–8.40)	7.90 (7.55–8.25)
	200	7.27 (6.87–7.68)	6.82 (6.27–7.38)	6.98 (6.59–7.37)	7.29 (7.01–7.57)
	400	7.08 (6.74–7.41)	6.83 (6.56–7.10)	7.38 (6.73–8.03)	7.30 (7.05–7.55)
	800	7.05 (6.69–7.42)	6.36 (6.13–6.59)	6.70 (6.29–7.11)	6.68 (6.51–6.86)
	1600	6.47 (6.27–6.67)	6.48 (6.15–6.82)	6.72 (6.17–7.28)	6.53 (6.35–6.71)
	All times	7.11 (6.95–7.27)	6.99 (6.74–7.24)	7.16 (6.92–7.41)	
New samples		8.96 (7.94-9.98)			

Numbers in brackets denote the confidence bounds (calculated using standard T-test).

TABLE IV
STANDARD DEVIATION OF BV (KV)

		Temperature (°C)			
		200	215	230	All temperatures
Time (h)	100	0.94 (0.73–1.32)	1.98 (1.54–2.77)	1.45 (1.13–2.03)	1.72 (1.51–2.01)
	200	0.93 (0.72–1.31)	1.30 (1.01–1.83)	0.90 (0.70–1.26)	1.37 (1.20–1.60)
	400	0.77 (0.60–1.09)	0.63 (0.49–0.89)	1.52 (1.18–2.15)	1.23 (1.08–1.44)
	800	0.80 (0.62–1.15)	0.54 (0.42–0.75)	0.97 (0.75–1.35)	0.82 (0.72–0.97)
	1600	0.43 (0.33–0.61)	0.83 (0.65–1.17)	0.78 (0.53–1.42)	0.68 (0.57–0.83)
	All times	0.86 (0.76–0.98)	1.39 (1.23–1.59)	1.25 (1.10–1.44)	
New samples		3.47 (2.88–4.36)			

Numbers in brackets denote the confidence bounds (calculated using F-test).

TABLE V
MEDIAN VALUES OF BV (KV)

		Temperature (°C)			
		200	215	230	245
Time (h)	100	7.59	7.71	7.12	7.69
	200	7.07	6.58	6.80	7.29
	400	6.99	6.65	6.84	7.13
	800	6.73	6.27	6.60	6.42
	1600	6.47	6.30	6.92	
New samples		9.26			

of new samples with histograms of BV measurements of samples aged for 100 and 1600 h in 200 °C. This result indicates that the significant spread of results for unaged samples is rather due to the material properties than the measurement method. Note that four BV measurements at four different points have been taken at each sample. However, the four outliers visible in Fig. 19 (i.e., BV measurement taken at unaged samples that are lower than 3 kV) have been measured at four different samples.

The BV has been modeled as a function of time using the following logarithmic relationship:

$$\mathrm{BV} = a - b \log_{10}(t - 1) \tag{2}$$

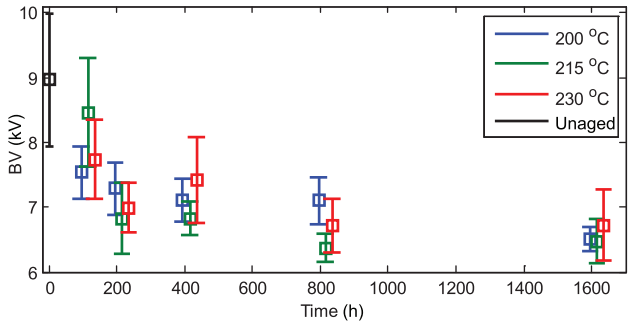

Fig. 18. BV measurements of insulation aged at different temperatures and times.

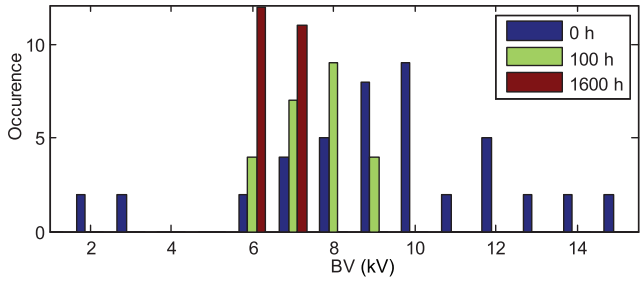

Fig. 19. Histograms of BV measurements of samples aged at 200 °C (for 100 and 1600 h) compared to histogram of BV measurements of unaged samples.

TABLE VI
PARAMETERS OF BV MODEL (2) AND THEIR CONFIDENCE BOUNDS

Temperature (°C)	a	b
200	9.262 ± 0.549	0.873 ± 0.247
215	9.262 ± 0.589	0.959 ± 0.247
230	9.218 ± 0.607	0.951 ± 0.286
All data	9.262 ± 0.421	0.896 ± 0.172

where BV (kV) denotes the breakdown voltage, t (h) denotes the time, and terms a and b are the model parameters. Since the distribution of BV measurements is not Gaussian and there are outliers in the data, parameters have been estimated using the median regression that is more robust to outliers as opposed to mean regression (i.e., the least squares method). Parameters of model (2) have been estimated for three different values of ageing temperature (i.e., 200 °C, 215 °C, and 230 °C). In addition, a fourth model that fits all the data (all temperatures) has been calculated. Parameters of the four cases of model (2) and their 95% confidence bounds (see [32] for more details) are presented in Table VI.

Modeled median values of BV for different temperatures are plotted in Fig. 20. The 95% confidence bounds of each model[4] have also been plotted. Although the differences in the BV models for different temperatures are not statistically significant (see large confidence bounds), the nominal models show that the ageing in 200 °C (solid blue line in Fig. 20) progresses more slowly than ageing at higher temperatures (i.e., 215 °C and 230 °C), which corresponds to the time evolution of material resistance observed in Figs. 10 and 14 (see Section V-B).

[4]Confidence bounds of median BV models plotted in Fig. 20 represent the most extreme cases of the parameters in Table VI.

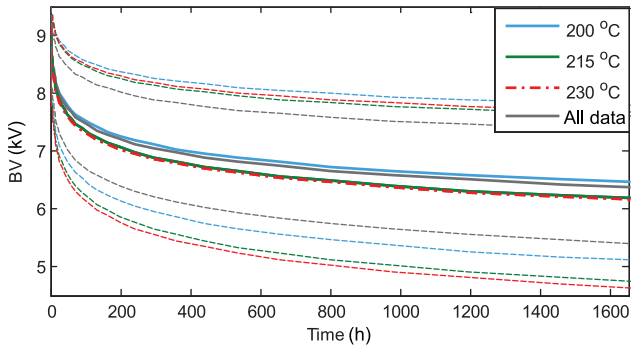

Fig. 20. Models of BV median for different values of ageing temperatures. Dashed lines of the respective colors denote the confidence bounds of the models.

VII. Conclusion and Future Work

Impact of ageing temperature and time on the electrical properties of the PAI insulation was analyzed. It is observed that during ageing at temperatures lower than or equal to 230 °C, the insulation resistance exhibits a particular trend: it decreases at first, followed by an increase after approximately 400 h. It also appears that this trend in material resistance is slightly slower for samples aged in 200 °C than for material aged in 215 °C and 230 °C. In addition, BV measurements lead to a similar conclusion—material ageing appears to progress more slowly in 200 °C.

On the contrary, while ageing at temperatures of 245 °C and higher, the insulation resistance rather increases, which may be an effect of delamination [31].

Furthermore, for almost all aged samples, the capacitance of the equivalent circuit model is lower than 20 pF, while the average capacitance of new samples is 22 pF.

Moreover, the study of new (unaged) insulation samples has been carried out for comparison purposes. The capacitance of new samples can be characterized by a single distribution with a mean value of 22.17 and a standard deviation of 2.46. The mean and median of BV of new samples is significantly higher than the one of aged material, which is an expected result. Interestingly, the standard deviation of BV measurements of new insulation is significantly higher than the standard deviation of BV measurements of aged samples.

References

[1] J. Tavner, "Review of condition monitoring of rotating electrical machines," *IET Elect. Power Appl.*, vol. 2, no. 4, pp. 215–247, 2008.

[2] H. O. Seinsch, "Monitoring und diagnose elektrischer Maschinen und Antriebe," in *Proc. VDE Workshop*, Allianz Schadensstattistik an HS Motoren, 2001, pp. 1996–1999.

[3] P. Zhang, Y. Du, T. G. Habetler, and B. Lu, "A survey of condition monitoring and protection methods for medium-voltage induction motors," *IEEE Trans. Ind. Appl.*, vol. 47, no. 1, pp. 34–46, Jan./Feb. 2011.

[4] P. O'Donnell, IEEE Motor Reliability Working Group, "Report of large motor reliability survey of industrial and commercial installations, Part I," *IEEE Trans. Ind. Appl.*, vol. IA-21, no. 4, pp. 853–864, Jul./Aug. 1985.

[5] P. O'Donnell, IEEE Motor Reliability Working Group, "Report of large motor reliability survey of industrial and commercial installations, Part II," *IEEE Trans. Ind. Appl.*, vol. IA-21, no. 4, pp. 865–872, Jul./Aug. 1985.

[6] P. O'Donnell, IEEE Motor Reliability Working Group, "Report of large motor reliability survey of industrial and commercial installations, Part III," *IEEE Trans. Ind. Appl.*, vol. IA-23, no. 1, pp. 153–158, Jan./Feb. 1985.

[7] R. M. Tallam *et al.*, "A survey of methods for detection of stator-related faults in induction machines," *IEEE Trans. Ind. Appl.*, vol. 43, no. 4, pp. 920–933, Jul./Aug. 2007.

[8] A. Bellini, F. Filippetti, C. Tassoni, and G. A. Capolino, "Advances in diagnostic techniques for induction machines," *IEEE Trans. Ind. Electron.*, vol. 55, no. 12, pp. 4109–4126, Dec. 2008.

[9] G. M. Joksimovic and J. Penman, "The detection of inter-turn short circuits in the stator windings of operating motors," *IEEE Trans. Ind. Electron.*, vol. 47, no. 5, pp. 1078–1084, Oct. 2000.

[10] K. N. Gyftakis and J. C. Kappatou, "The zero-sequence current as a generalized diagnostic mean in Δ-connected three-phase induction motors," *IEEE Trans. Enery Convers.*, vol. 29, no. 1, pp. 138–148, Mar. 2014.

[11] C. Gerada *et al.*, "The results do mesh," *IEEE Ind. Appl. Mag.*, vol. 13, no. 2, pp. 62–72, Mar./Apr. 2007.

[12] S. Williamson and K. Mirzoian, "Analysis of cage induction motors with stator winding faults," *IEEE Trans. Power App. Syst.*, vol. PAS-104, no. 7, pp. 1838–1842, Jul. 1985.

[13] A. J. M. Cardoso, S. M. A. Cruz, and D. S. B. Fonseca, "Inter-turn stator winding fault diagnosis in three-phase induction motors, by Park's vector approach," *IEEE Trans. Energy Convers.*, vol. 14, no. 3, pp. 595–598, Sep. 1999.

[14] J. F. Martins, V. F. Pires, and A. J. Pires, "Unsupervised neural-network-based algorithm for an on-line diagnosis of three-phase induction motor stator fault," *IEEE Trans. Ind. Electron.*, vol. 54, no. 1, pp. 259–264, Feb. 2007.

[15] S. M. A. Cruz and A. J. M. Cardoso, "Stator winding fault diagnosis in three-phase synchronous and asynchronous motors, by the extended Park's vector approach," *IEEE Trans. Ind. Appl.*, vol. 37, no. 5, pp. 1227–1233, Sep./Oct. 2001.

[16] A. M. da Silva, R. J. Povinelli, and N. A. O. Demerdash, "Induction machine broken bar and stator short-circuit fault diagnostics based on three-phase stator current envelopes," *IEEE Trans. Ind. Electron.*, vol. 55, no. 3, pp. 1310–1318, Mar. 2008.

[17] M. Drif and A. J. M. Cardoso, "Stator fault diagnostics in squirrel cage three-phase induction motor drives using the instantaneous active and reactive power signature analyses," *IEEE Trans. Ind. Informat.*, vol. 10, no. 2, pp. 1348–1360, May 2014.

[18] A. S. Babel and E. G. Strangas, "Condition-based monitoring and prognostic health management of electric machine stator winding insulation," in *Proc. IEEE Int. Conf. Elect. Mach. (ICEM)*, Berlin, Germany, Sep. 2014, pp. 1855–1861.

[19] G. C. Stone, E. A. Boulter, I. Culbert, and H. Dhirani, "Electrical insulation for rotating machines-design, evaluation, aging, testing and repair," *IEEE Elect. Insul. Mag.*, vol. 20, no. 3, p. 65, May/Jun. 2004.

[20] A. J. Gonzalez, M. S. Baldwin, J. Stein, and N. E. Nilsson, *Monitoring and Diagnosis of Turbine-Driven Generators*. Englewood Cliffs, NJ, USA: Prentice-Hall, 1995.

[21] I. Culbert, H. Dhirani, and G. C. Stone, *Handbook to Assess the Insulation Condition of Large Rotating Machines*, vol. 16, Palo Alto, CA, USA: Electric Power Res. Inst., 1989.

[22] K. Younsi, P. Neti, M. Shah, J. Y. Zhou, J. Krahn, and K. Weeber, "On-line capacitance and dissipation factor monitoring of ac stator insulation," *IEEE Trans. Dielect. Elect. Insul.*, vol. 17, no. 5, pp. 1441–1452, Oct. 2010.

[23] M. Farahani, E. Gockenbach, H. Borsi, K. Schäfer, and M. Kaufhold, "Behavior of machine insulation systems subjected to accelerated thermal aging test," *IEEE Trans. Dielect. Elect. Insul.*, vol. 17, no. 5, pp. 1364–1372, Oct. 2010.

[24] N. Lahoud, J. Faucher, D. Malec, and P. Maussion, "Electrical aging of the insulation of low-voltage machines: Model definition and test with the design of experiments," *IEEE Trans. Ind. Electron.*, vol. 60, no. 9, pp. 4147–4155, Sep. 2013.

[25] S. Savin, S. Ait-Amar, and D. Rogers, "Cable aging influence on motor diagnostic system," *IEEE Trans. Dielect. Elect. Insul.*, vol. 20, no. 4, pp. 1340–1346, Aug. 2013.

[26] F. Salameh, A. Picot, M. Chabert, E. Leconte, A. Ruiz-Gazen, and P. Maussion, "Variable importance assessment in lifespan models of insulation materials: A comparative study," in *Proc. 10th IEEE Int. Symp. Diagn. Elect. Mach. Power Electron. Drives (SDEMPED)*, Guarda, Portugal, Sep. 2015, pp. 198–204.

[27] C. Zoeller, M. A. Vogelsberger, R. Fasching, W. Grubelnik, and T. M. Wolbank, "Evaluation and current-response based identification of insulation degradation for high utilized electrical machines in railway application," in *Proc. 10th IEEE Int. Symp. Diagn. Elect. Mach. Power Electron. Drives (SDEMPED)*, Guarda, Portugal, Sep. 2015, pp. 266–272.
[28] S. Thomas, K. Joseph, S. K. Malhotra, K. Goda, and M. S. Sreekala, *Polymer Composites Volume 1: Macro- and Microcomposites*. Hoboken, NJ, USA: Wiley, 2012.
[29] A. Hulme and J. Cooper, "Life prediction of polymers for industry," *Seal. Technol.*, vol. 2012, no. 9, pp. 8–12, Sep. 2012.
[30] R. Morin and R. Bartnikas, "Multistress aging of stator bars in a three-phase model stator under load cycling conditions," *IEEE Trans. Energy Convers.*, vol. 27, no. 2, pp. 374–381, Jun. 2012.
[31] K. N. Gyftakis, M. Sumislawska, D. F. Kavanagh, D. Howey, and M. McCulloch, "Dielectric characteristics of electric vehicle traction motor's winding insulation under thermal ageing," *IEEE Trans. Ind. Appl.*, vol. 52, no. 2, pp. 1398–1404, Mar./Apr. 2016.
[32] L. Ljung, *System Identification: Theory for the User*. Englewood Cliffs, NJ, USA: Prentice-Hall, 1999.
[33] M. H. DeGroot and M. J. Schervish, *Probability and Statistics*, 4th ed., Pearson Education, 2002.

Malgorzata Sumislawska received the M.Sc. degree in teleinformatics from Wroclaw University of Technology, Wroclaw, Poland, in 2009, and the M.Sc. degree in systems and control and the Ph.D. degree in mathematics and control engineering from Coventry University (CU), Coventry, U.K., in 2009 and 2012, respectively.

She is currently a Lecturer of System Identification with CU. Her research interests include fault detection and diagnosis, data-based reduced -order modeling for control diagnostics and prognostics, state and parameter estimation, and filtering.

Konstantinos N. Gyftakis (M'11) was born in Patras, Greece, in May 1984. He received the Diploma degree in electrical and computer engineering and the Ph.D. degree in electrical machines condition monitoring and fault diagnosis from the University of Patras, Patras, Greece, in 2010 and 2014, respectively.

He was a Post-Doctoral Research Assistant with the Department of Engineering Science, University of Oxford, Oxford, U.K. He is currently a Lecturer with the Faculty of Engineering, Environment, and Computing, Coventry University, Coventry, U.K. He has authored/coauthored more than 30 papers published in international scientific journals and conference proceedings. His research interests include fault diagnosis, condition monitoring, and degradation of electrical machines.

Darren F. Kavanagh received the Ph.D. degree I in advanced signal processing and pattern recognition for acoustic signals from Trinity College Dublin, Dublin, Ireland, in 2011.

He is an Assistant Lecturer with the Institute of Technology Carlow, Carlow, Ireland. He was a Post-Doctoral Researcher with the University of Oxford, Oxford, U.K., investigating the area of degradation and failure analysis of electric machines with specific applications in electric vehicles. He has gained valuable academic experience at educational institutions such as the University of Oxford; Trinity College Dublin; and the Institute of Technology Tallaght, Dublin, Ireland. He has also benefited greatly from industrial experience at Alcatel Lucent-Bell Laboratories, Intel, and Xilinx.

Dr. Kavanagh was awarded an EMBARK Scholarship in 2006 by the Irish Research Council to pursue a Ph.D. degree in acoustic signal processing. He was the recipient of the prestigious Minister's Silver Medal for Science from the Minister for Education (Ireland) in 2004.

Malcolm D. McCulloch (S'88–M'89) was born in South Africa. He received the B.Sc.(Eng.) and Ph.D. degrees in electrical engineering from the University of Witwatersrand, Johannesburg, South Africa, in 1986 and 1990, respectively.

In 1993, he moved to start up the Electrical Power Group at Oxford University, Oxford, U.K., where he is currently an Associate Professor. The group's focus is to develop and commercialize sustainable energy technologies in the four sectors of energy for development, domestic energy use, transport, and renewable generation. His work addresses transforming existing power networks, designing new power networks for the developing world, developing new technology for electric vehicles, and developing approaches to integrated mobility. He has more than 100 journal and refereed conference papers, 15 patents, and 4 spinout companies.

Keith J. Burnham received the B.Sc., M.Sc., and Ph.D. degrees in 1981, 1984, and 1991, respectively.

He was a Founding Member of the Control Theory and Applications Centre in 1987, and has been a Professor of Industrial Control Systems since 1999. His research interests include self-tuning and adaptive control for nonlinear industrial systems, with particular interest in bilinear systems. Strong collaboration involves consultancy with a wide range of industrial organizations, research with international academic organizations, as well as an active involvement with the major U.K. professional bodies.

David A. Howey (M'10) received the B.A. degree and the M.Eng. degree in electrical and information sciences from Cambridge University, Cambridge, U.K., in 2002, and the Ph.D. degree in electrical machines from Imperial College London, London, U.K., in 2010.

He is currently an Associate Professor with the Energy and Power Group, Department of Engineering Science, University of Oxford, Oxford, U.K. He leads projects on fast electrochemical modeling, model-based battery management systems, battery thermal management, and motor degradation. His research interests include condition monitoring and management of electric and hybrid vehicle components.